Mon. Not. R. Astron. Soc. **305,** 231–240 (1999)

X-ray spectral evolution of GS 2023+338 (V404 Cyg) during decline after outburst

Piotr T. Życki,[1,3]⋆ Chris Done[1]⋆ and David A. Smith[2]†

[1] *Department of Physics, University of Durham, South Road, Durham DH1 3LE*
[2] *Department of Physics and Astronomy, University of Leicester, University Road, Leicester LE1 7RH*
[3] *Nicolaus Copernicus Astronomical Center, Bartycka 18, 00-716 Warsaw, Poland*

Accepted 1998 December 22. Received 1998 November 9; in original form 1998 August 12

ABSTRACT

We have reanalysed archival *Ginga* data of the soft X-ray transient source GS 2023+308 (V404 Cyg) covering the decline phase of its 1989 May outburst. Our spectral modelling includes the relativistically smeared Compton-reflected continuum and iron Kα fluorescent line near 6.5 keV produced by X-ray illumination of the accretion disc. This gives a powerful diagnostic of the accretion geometry, with the amplitude of the reprocessed components showing the solid angle subtended by the disc, while the detailed shape of the relativistic smearing shows how close this material is to the black hole event horizon.

We find that reflection is always significantly present in the spectra, but that its fractional contribution decreases as the decline progresses. The amount of relativistic smearing is also consistent with decreasing during the decline, although this is poorly constrained except for the brightest spectra. One plausible scenario explaining this evolution is of an optically thick disc with inner radius increasing as a function of time, with the X-ray source in the form of a central corona. This is similar to the evolution inferred for other X-ray transient sources, such as Nova Muscae, except that the underlying power-law spectrum of GS 2023+338 stayed constant as the disc geometry changed. This challenges the underlying assumption of almost all models for the spectra of accreting black holes, namely that the hard X-rays are formed by Comptonization of seed photons from the accretion disc.

Key words: accretion, accretion discs – black hole physics – stars: individual: GS 2023+338 – X-rays: stars.

1 INTRODUCTION

The 'no hair' theorem for black holes states that they can be described solely in terms of their mass and spin (and charge, although this is unlikely to be important in physically realistic situations). Black holes are then completely characterized by two parameters, making them much less complex than e.g. neutron stars, where there can be a strong magnetic field, and where there is an uncertain equation of state for the dense material. Black hole binary systems are then the simplest objects in which to study the physics of accretion flows in strong gravity, and have the further advantage that the orbital parameters are often well studied so that the inclination, mass and distance of the system are tightly constrained.

Many of the black hole binary systems show dramatic outbursts where the luminosity rises rapidly from a very faint quiescent state to one which is close to the Eddington limit, $L_{\rm Edd}$, and then declines approximately exponentially over a period of months. These systems are the soft X-ray transients (hereafter SXT; see Tanaka & Lewin 1995, Tanaka & Shibazaki 1996 for reviews), with the outburst triggered by the classic disc instability, which occurs as hydrogen starts to become partially ionized (Meyer & Meyer-Hofmeister 1981; Smak 1982; see Osaki 1996 for review). The dramatic increase in mass-accretion rate on to the central object gives rise to strong X-ray emission. This illuminates the disc, and controls its evolution during the decline phase (King & Ritter 1998; King 1998), and in quiescence (King, Kolb & Szuszkiewicz 1997).

The SXT also show spectral evolution during the outburst and decline. In general, when the luminosity is close to the Eddington limit, their X-ray spectra show a strong thermal component at $\sim$1 keV, accompanied by a strongly variable power law (very high or flare state). As the luminosity decreases then the power-law component decreases in importance, giving the high or soft state, which is dominated by the thermal component. There is then a marked transition at $L \sim 0.1 L_{\rm Edd}$ as the thermal component decreases in both luminosity and temperature, and a hard, strongly

⋆E-mail: ptz@camk.edu.pl (PTZ); chris.done@durham.ac.uk (CD)
†Present address: NASA/Goddard Space Flight Center, Greenbelt, MD 20771, USA.

variable power law dominates the X-ray spectrum (the low or hard state). This spectrum remains fairly stable to very low luminosities, where the source is in the quiescent or off state (Miyamoto et al. 1992; Nowak 1995; Tanaka & Lewin 1995; Tanaka & Shibazaki 1996).

According to current paradigm the thermal component originates in an optically thick accretion disc for which the Shakura–Sunyaev (1973; hereafter SS) solution is commonly used, while the hard power law is produced by hot, optically thin plasma. The geometry inferred for the low/hard state from modelling the broad-band (1–200 keV) spectrum of both transient and persistent sources (Dove et al. 1997; Gierliński et al. 1997a; Poutanen, Krolik & Ryde 1997; see Poutanen 1998 for a review) is that of a geometrically thin, cool accretion disc that truncates at some transition radius, $r_{\rm tr}$, which is rather larger than the innermost stable orbit at $6R_{\rm g}$ ($R_{\rm g} \equiv GM/c^2$), with the inner region filled by a quasi-spherical, X-ray hot plasma.

Another independent diagnostic of the accretion geometry is produced as the X-rays illuminate the disc. An iron fluorescence line and reflected continuum are formed wherever hard X-rays illuminate optically thick material (George & Fabian 1991; Matt, Perola & Piro 1991), but around a black hole these spectral features should be strongly smeared by the combination of Doppler effects from the high orbital velocities and strong gravity (Fabian et al. 1989). Modelling of the detailed shape of this relativistic smearing directly constrains the distance of the cool reflecting material from the black hole, while the amount of reflection and line constrains the geometry. Results from this approach from low-state spectra of both transient and persistent Galactic black hole binaries are consistent with the geometry described above (Ueda, Ebisawa & Done 1994; Ebisawa et al. 1994; Życki, Done & Smith 1997, hereafter Paper I; Życki, Done & Smith 1998, hereafter ZDS98; Done & Życki 1998).

The inferred high state geometry is rather different. Both broad-band spectra and detailed modelling of the reprocessed component give a consistent picture in which the optically thick disc extends all the way down to the last stable orbit (Poutanen et al. 1997; Gierliński et al. 1997b; ZDS98; Cui et al. 1997). The transition to the high state then seems to involve a decrease of $r_{\rm tr}$ and consequently an increase of the disc thermal emission at the expense of the power-law component. Further evolution to the very high state presumably requires a redistribution of the energy generation so that the relative contribution of a coronal source increases.

There is no current model able to explain compellingly all this evolution. Perhaps the best to date is that of Esin, McClintock & Narayan (1997), who go some way towards constructing the global dynamics as a function of mass-accretion rate. At low mass-accretion rates there are at least two thermally and viscously stable solutions of the accretion flow. One is the familiar optically thick, geometrically thin, SS disc, where the energy released is efficiently radiated via blackbody cooling. Another is a hot, optically thin, geometrically thick flow in which the radiative cooling is rather inefficient so that radial energy transport (advection) is important (advection-dominated accretion flows, hereafter ADAF; see e.g. the review by Narayan 1997). For the hot solution, an increasing mass-accretion rate, $\dot{m}$ means that the flow density and, consequently, its radiative efficiency increases. Eventually, at some critical accretion rate $\dot{m} = \dot{m}_{\rm crit}$, the cooling becomes efficient enough to collapse the hot solution down into an SS disc. Esin et al. (1997) calculate that this transition occurs for luminosities $\sim 0.08 L_{\rm Edd}$, so they identify the low–high state change with the infalling material switching from an ADAF to SS disc.

At least three of the currently known transient black hole systems did not show this canonical behaviour. GS 2023+338 (V404 Cyg), GRO J0422+32 (Nova Persei 1992) and GRS 1716−249 (Nova Oph 1993) remained dominated by the non-thermal component throughout the entire decline phase. For GRO J0422+32 and GRS 1716−29 this is plausibly because the system luminosities were never higher than $\sim 0.1 L_{\rm Edd}$ so that it never went above the low state (Nowak 1995; Esin et al. 1998; Revnivtsev et al. 1998), but this is clearly not the case for GS 2023+338, where the luminosity almost reached the Eddington limit (Tanaka & Lewin 1995). This system is especially interesting as it was used as an example for the ADAF-based models of SXTs in quiescence (Narayan, Barret & McClintock 1997), yet its outburst behaviour is apparently very different from that predicted by the extension of this model to the overall evolution of SXT (Esin et al. 1997).

In this paper we present results of detailed spectral analysis of data obtained during the 1989 outburst of GS 2023+338 (Kitamoto et al. 1989), and use the relativistically smeared reprocessed component to constrain the accretion geometry. The outburst was well covered by *Ginga* from its first detection by the All Sky Monitor on 1989 May 22 until November (Tanaka & Lewin 1995). In this paper we concentrate on the decline phase of the outburst after 1989 June 1, leaving detailed discussion of the most dramatic 'day in the life' of GS 2023+338 (May 30) to a forthcoming paper. For our analysis we have selected several data sets when the effect of photoelectric absorption (another unusual feature of the source) was small and we aim at describing the evolution with the accretion flow geometry in the vicinity of the central black hole. We then compare this evolution with more typical cases of STX e.g. Nova Muscae 1991, and with the predictions of the Esin et al. (1997) model.

2 DATA REDUCTION AND BACKGROUND SUBTRACTION

The data were extracted from the original first reduction files in the usual manner using the *Ginga* reduction software at Leicester University. However, unlike most X-ray sources, the spectrum of GS 2023+338 contributes a significant number of counts above 24 keV. This count rate is used as a background monitor (surplus above upper discriminator, or SUD), but here it is contaminated by the source. The SUD rate minus the contribution from the source was estimated from off-source data taken before and after the source observation. We are able to do this because the satellite position in orbit, and thus the intrinsic background, depends on two parameters (excluding the phase of the 37-day orbital period of *Ginga*): the angle from the ascending node of the orbit and the longitude of the ascending node (K. Hayashida, private communication). We mapped the SUD rate from the uncontaminated observations against both orbital parameters (dividing the data into 20 degree bins). For each data point from the observation of the source we calculated the orbital parameters and replaced the contaminated SUD value with that from the corresponding orbital parameters on the uncontaminated grid. We can then perform either a 'local' or 'universal' background subtraction as normal (Hayashida et al. 1989). We chose the universal background since there were no background observations suitable for the local method.

To test the method we used the off-source (uncontaminated) data using both the original and modified SUD values. The rms deviations of the resulting spectra were less than 5–7 per cent over the 2–20 keV range. Secondly, we performed a similar analysis on MCG-2-58-22 (1989 Nov. observation), comparing the 'universal' background subtraction before and after inserting modified SUD

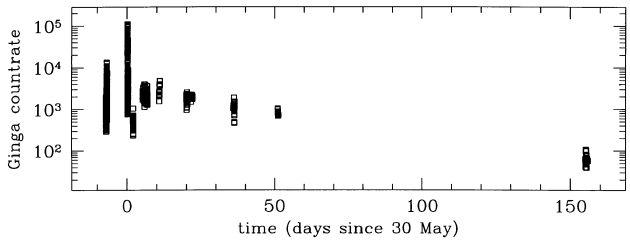

Figure 1. *Ginga* light curve (1–20 keV) of GS 2023+338 since the first pointed observations on 1989 May 23 until 1989 November. The count rate was corrected for background, deadtime and aspect. Dramatic flux and spectral variability was observed on May 30. Flux variability occurred during each observation but the degree of spectral variability was changing with time. The upper envelope of the light curve (the May 23 and 30 points excepted) follows an approximately exponential decline with e-folding time ~40 d.

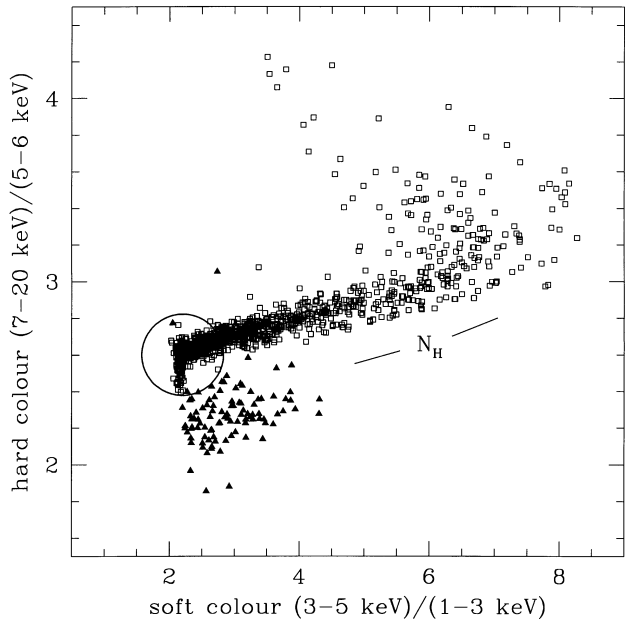

Figure 2. The colour–colour diagram of GS 2023+338 using the decline phase data i.e. after 1989 June 1. The well-defined (almost) horizontal track is due to photoelectric absorption with N_H increasing to the right. The turn-off point corresponds to $N_H \sim 4 \times 10^{23}$ cm^{-2}, when the spectrum above 5 keV begins to be affected. The circle marks a region where the June – July data for detailed spectral analysis were extracted from. The November data are those marked with filled triangles (see Table 1).

values. The results from the real and modified SUD data were in agreement within the error bars, showing that the method is reliable.

3 DATA SELECTION FOR SPECTRAL ANALYSIS

The variability characteristics of these data were examined in detail by Oosterbroek et al. (1996, 1997). Here we show the light curves (Fig. 1) and colour–colour diagram (Fig. 2) for completeness. There is remarkable variability both in flux and in spectral shape (see also Tanaka & Lewin 1995). Oosterbroek et al. (1997) showed that the well-defined track (marked N_H on Fig. 2) is consistent with being the result of increasing photoelectric absorption. The left-hand side of this track seems to end at a well-defined point, plausibly because this represents the unabsorbed primary spectrum. We extracted data sets from this point in order to try to constrain the underlying spectral shape since the beginning of June to the last *Ginga* observation in 1989 (November), as detailed in Table 1.

4 MODELS

We use a variety of models for the data analysis. The soft component is described by a blackbody or a disc blackbody (i.e. multitemperature composition of blackbody spectra; Frank, King & Raine 1992; Mitsuda et al. 1984). For the hard component we use a power law, and its reflected continuum is modelled using the angle-dependent Green's functions of Magdziarz & Zdziarski (1995) as implemented in the `pexriv` model in XSPEC spectral analysis package (Arnaud 1996). This calculates the ionization state of the material by balancing photoelectric ionization from the irradiating hard power law against radiative recombination, as in Done et al. (1992). The photoelectric absorption edge energies for iron were corrected from the rather approximate values given by Reilman & Manson (1979) to those of Kaastra & Mewe (1993). The recombination rate is a function of temperature, while the photoionization rate depends on the ionization parameter $\xi = L_X/nr^2$ where L_X is the ionising luminosity, n is the density of the reflector and r is the distance of the reflector from the X-ray source. At a given temperature (which is chosen rather than calculated self-consistently in this code) then the ion populations are determined by ξ, with a rather weak dependence on the spectral shape (see Done et al. 1992).

The iron Kα line corresponding to a given ionization state, plasma temperature and spectral shape is computed self-consistently in our code, rather than modelled as a separate component. We use the Monte Carlo code of Życki & Czerny (1994) to compute the line intensity and profile (which is broadened by Compton scattering in the reflector and a possible range of ionization stages of iron). The line is then added to the reflected continuum to give the total reprocessed spectrum.

This total reprocessed spectrum can then be corrected for relativistic and kinematic effects, which cause 'smearing' of spectral features (e.g. Fabian et al. 1989). These effects are calculated for a monochromatic line in the XSPEC `diskline` model so we use this, modified to include the light bending effect in Schwarzschild geometry, to calculate the spectral smearing, and convolve this with the total reprocessed spectrum. The `diskline` model is parametrized by the inner and outer radii of the reflecting accretion disc, R_{in} and R_{out}, radial distribution of irradiation emissivity for which we assume $F_{irr}(r) \propto r^{\beta}$ and the inclination of the disc, i. In our basic models we assume $R_{out} = 10^4 R_g$ and $\beta = -3$ (see Appendix A) and fit R_{in} and the amplitude of the reprocessed component expressed as the solid angle of the reprocessor as seen from the X-ray source normalized to 2π i.e. $\Omega_r \equiv \Omega/2\pi$ (so that $\Omega_r = 1$ corresponds to an isotropic source located above a flat, infinite disc). This means that we do not assume any specific geometry that would result in a unique relation between R_{in}, R_{out}, β and Ω_r. The models will be referred to as `relrepr` hereafter.

We assume cosmic abundances of Morrison & McCammon (1983) with the possibility of a variable iron abundance in the reprocessor; we fix the inclination of the source at $i = 56^\circ$ and assume the mass of the black hole is 12 $M_\odot$ (Shahbaz et al. 1994).

The spectral analysis was performed using XSPEC version 10 (Arnaud 1996) into which all the non-standard models mentioned above were implemented as local models.

Table 1. Observations log for analysis of unabsorbed, decline phase spectra.

Label	Data set	Start date/time	End date/time	Start date−May 30 (d)	Exposure (s)
1.	June 3.	89/154 3/06 16:36:31	3/06 16:43:27	4	416
2.	June 4.	89/155 4/06 12:11:59	4/06 12:20:07	5	488
3.	June 10.	89/161 10/06 01:58:00	10/06 02:15:04	11	1024
4.	June 19.	89/170 19/06 06:29:40	19/06 07:46:40	20	1900
5.	June 20.	89/171 20/06 14:05:00	21/06 04:00:00	21	12180
6.	July 6.	89/187 6/07 09:47:00	6/07 10:10:28	37	1408
7.	July 20.	89/201 20/07 01:00:00	22/07 05:13:00	51	7650
8.	November	89/305 1/11 00:20:00	1/11 22:00:00	155	19064

Table 2. Results of model fitting to the sequence of decline phase spectra.

Label	$N_{\rm H}$	$kT_{\rm soft}$ (keV)	$D_{\rm in}$ ($R_{\rm g}$)	Γ	N	$\Omega_{\rm r}$	ξ	$R_{\rm in}$ ($R_{\rm g}$)	χ^2/d.o.f.
1.	1.73 ± 0.22	$0.22^{+0.06}_{-0.09}$	$11^{+\infty}_{-9}$	1.67 ± 0.03	$1.42^{+0.09}_{-0.07}$	$0.70^{+0.12}_{-0.10}$	$0.1^{+2}_{-0.1}$	20^{+20}_{-9}	18.6/23
2.	$1.54^{+0.26}_{-0.20}$	$0.24^{+0.07}_{-0.10}$	7^{+82}_{-4}	1.70 ± 0.03	$1.21^{+0.07}_{-0.06}$	$0.83^{+0.13}_{-0.11}$	$0.1^{+2}_{-0.1}$	30^{+60}_{-11}	21.6/23
3.	$1.75^{+0.22}_{-0.24}$	$0.27^{+0.03}_{-0.04}$	8^{+5}_{-3}	1.76 ± 0.03	$2.35^{+0.10}_{-0.13}$	$0.88^{+0.12}_{-0.10}$	$0^{+0.1}$	17^{+9}_{-5}	21.3/23
4.	$2.04^{+0.22}_{-0.26}$	0.295 ± 0.010	$5.4^{+1.2}_{-1.1}$	1.72 ± 0.03	1.16 ± 0.06	$0.66^{+0.11}_{-0.07}$	0^{+1}	18^{+13}_{-7}	23.1/23
5.	$1.28^{+0.30}_{-0.34}$	$0.37^{+0.12}_{-0.04}$	$1.6^{+1.0}_{-1.3}$	1.67 ± 0.03	$0.93^{+0.05}_{-0.06}$	0.50 ± 0.08	$1^{+8}_{-0.9}$	36^{+80}_{-17}	7.85/23
6.	$2.05^{+0.22}_{-0.33}$	$0.23^{+0.04}_{-0.07}$	9.5^{+32}_{-4}	1.64 ± 0.03	0.67 ± 0.04	0.47 ± 0.09	1^{+9}_{-1}	$80^{+\infty}_{-55}$	22.8/23
7.	$1.19^{+0.36}_{-0.25}$	$0.43^{+0.22}_{-0.07}$	$0.6^{+0.7}_{-0.5}$	1.70 ± 0.03	0.39 ± 0.03	0.37 ± 0.07	12^{+30}_{-8}	$60^{+\infty}_{-35}$	19.9/23
8.	3.3 ± 0.6	$0.30^{+0.04}_{-0.15}$	$1^{+8}_{-0.4}$	1.93 ± 0.05	$(5.4^{+0.6}_{-0.4}) \times 10^{-2}$	$0.36^{+0.16}_{-0.10}$	60^{+90}_{-45}	$600^{+\infty}_{-565}$	26.3/22

$N_{\rm H}$ – hydrogen column of uniform absorber in units of 10^{22} cm^{-2}.
$D_{\rm in}$ – inner radius of emitting disc as found from the amplitude of the soft thermal component.
Γ – photon index of the primary power law.
N – normalization of the primary power law (photons/cm^2/s/keV).
$\Omega_{\rm r}$ – amplitude of the smeared, reprocessed component.
ξ – ionization parameter, $L_{\rm X}/nr^2$.
$R_{\rm in}$ – inner radius of the disc as found from the magnitude of the relativistic effects.

5 RESULTS

The primary spectrum of the source is consistent with a simple power law after June 1 (MJD−47 000 = 677), so we can use this, together with the `relrepr` model and a soft component (disc blackbody) to describe the data. We assumed our basic reprocessing model, i.e. only one reprocessed component (cf. Section 6.1), with ionization and relativistic smearing allowed for. We fix $R_{\rm out}$ at $10^4\,R_{\rm g}$ and $F_{\rm irr}(r) \propto r^{-3}$ and we fit the amplitude $\Omega_{\rm r}$, the inner radius $R_{\rm in}$ and the ionization parameter ξ. Results of the spectral modelling are presented in Table 2 and the spectra are plotted in Fig. 3.

The reprocessed component is significantly present in all data sets. It is very weakly ionized, and generally significantly smeared although not to the extent expected for a disc extending down to the last stable orbit at $6\,R_{\rm g}$. We note that the two effects (ionization and relativistic smearing) can be separated given good quality data. The basic reason for this is that the ionization broadens the spectral features towards higher energy whilst the relativistic effects smear them around their rest-frame energy. Secondly, the strength of the Fe spectral features increases dramatically with ionization whilst relativistic effects only redistribute the photons. Fig. 4 illustrates the above discussion showing that there is no correlation between ξ and $R_{\rm in}$, even if a radial distribution of ionization is assumed.

Fig. 5a shows how the amplitude of the reflected component decreases during the decline phase. Initially, the amplitude of reflection is close to unity i.e. the cold, optically thick disc covers $\sim 2\pi$ solid angle as seen from the X-ray source, but this drops significantly as the source luminosity fades. The inner disc radius derived from the amount of relativistic smearing is always incompatible with the last stable orbit in a Schwarzschild metric of $R_{\rm ms} = 6\,R_{\rm g}$ (although with the caveat that $R_{\rm in}$ is correlated with the form of irradiation emissivity). The inner disc radius is consistent with being anticorrelated with the amount of reflection, although the change in the amount of smearing is only marginally significant.

These results agree with and extend those obtained in Paper I, where only a subset of present data was analysed. They confirm that optically thick accretion material (the putative accretion disc) was present in the system throughout the decline, even though the source luminosity is clearly dominated by the power-law component, rather than by direct thermal emission from the disc.

6 COMPARISON WITH OTHER SXTs

The trend we see in the data of a gradual decrease of $\Omega_{\rm r}$ possibly correlated with increasing $R_{\rm in}$ is similar to that previously found in another SXT source, Nova Muscae 1991 (ZDS98, fig. 2). However, there is a marked difference in the *spectral* evolution of GS 2023+338 compared to Nova Muscae. The spectral index of the primary spectrum of GS 2023+338 stayed roughly constant during the decline phase, except for the last data set (November) obtained 5 months after the outburst, when the power law was significantly softer than during the first two months. Conversely, in Nova Muscae we found a monotonic decrease of Γ (hardening of the spectrum) with time, correlated with decreasing $\Omega_{\rm r}$ and increasing

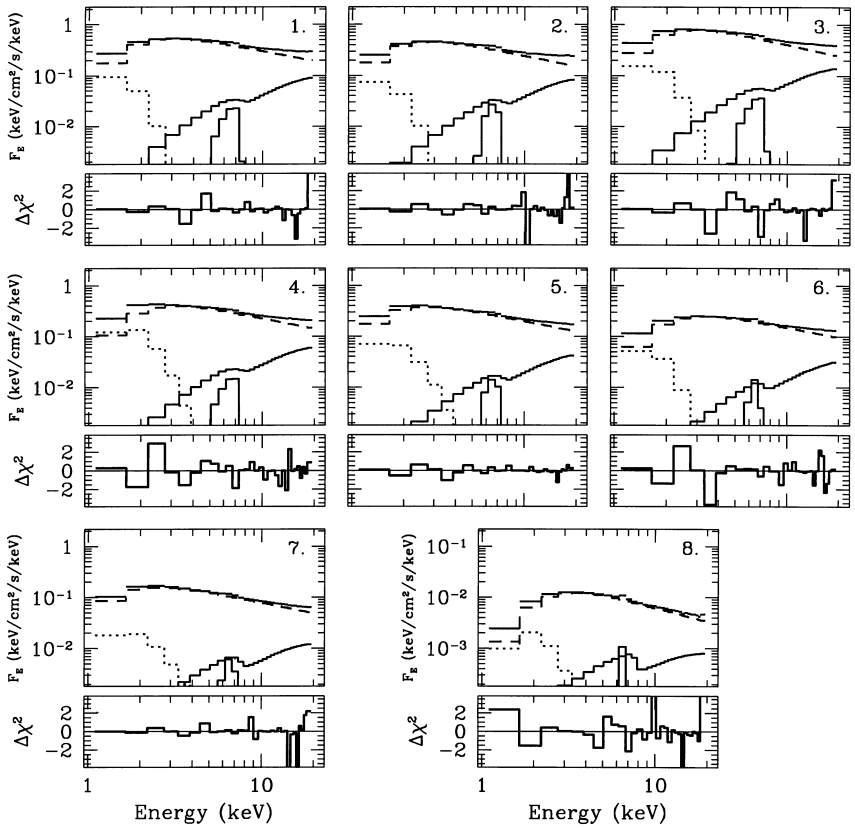

Figure 3. Unfolded spectra of the source (upper box in each panel) and χ^2 residuals (lower boxes) for all data sets. Labels in upper right corners refer to given data set (Table 2). Data points are plotted with (invisible) error bars. The solid histograms show the reprocessed component; the Fe Kα line and the Compton-reflected continuum are separated for plotting only. The dashed histograms are the primary power laws while the dotted histograms show the soft thermal component. Note that the flux scale in the last panel (8) is shifted down by a factor of 10.

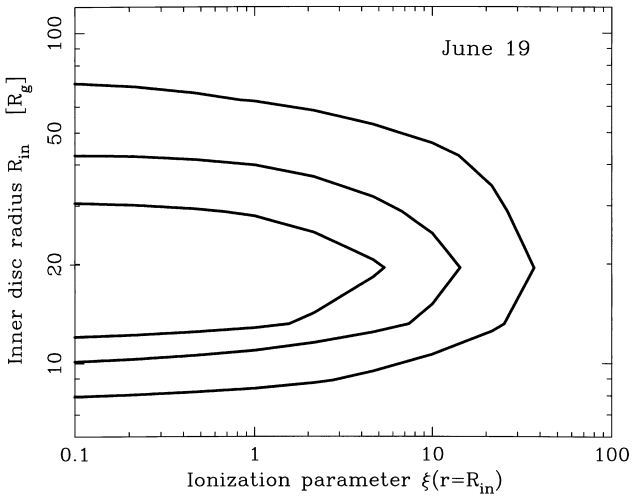

Figure 4. This plot demonstrates that the effects of relativistic smearing and broadening owing to multiple ionization *can* be separated in our model. It shows contours of $\Delta\chi^2 = 2.3,\ 4.6$ and 9.2 as a function of the inner disc radius R_{in} and the ionization parameter $\xi(r = R_{in})$ (assuming $\xi(r) \propto r^{-4}$) for the June 19 data set. The best fit has low ionization ($\xi \sim 0.1$) and $R_{in} \sim 20$, and there is no correlation between the two parameters.

R_{in} (see Fig. 6; ZDS98). A similar correlation between Ω_r and Γ is also seen from GX339-4 (Ueda et al. 1994; Fig. 6)

The results from Nova Muscae and GX339-4 can be understood in terms of a phenomenological scenario where a retreating disc (increasing R_{in}) gives a smaller solid angle for reflection and a diminishing supply of soft photons for Comptonization, so leading to a harder X-ray continuum spectrum (Esin et al. 1997; ZDS98). The lack of such a correlation in GS 2023+338 is then a clear problem, implying that the observed change in solid angle for the reflecting material does not give rise to a change in the ratio of soft seed photons available for Compton scattering, i.e. that the observed reflecting material is not the dominant source of soft seed photons for the Comptonization that gives rise to the hard power law. It is rather hard to imagine how this can be the case. If there is another soft seed photon contribution, perhaps from stronger cyclo/synchrotron emission, then the expected behaviour would be that the hard X-ray source would have a softer spectral index. GS 2023+338 instead shows a rather hard spectral index at all times. Perhaps a better explanation is that there is an additional contribution to the reflected component from more distant, cold material, which does not then contribute much to the soft seed photons impinging on the X-ray source. We will now investigate such additional reprocessed components.

6.1 Additional sites of reprocessing

Additional material around the source is clearly present, as

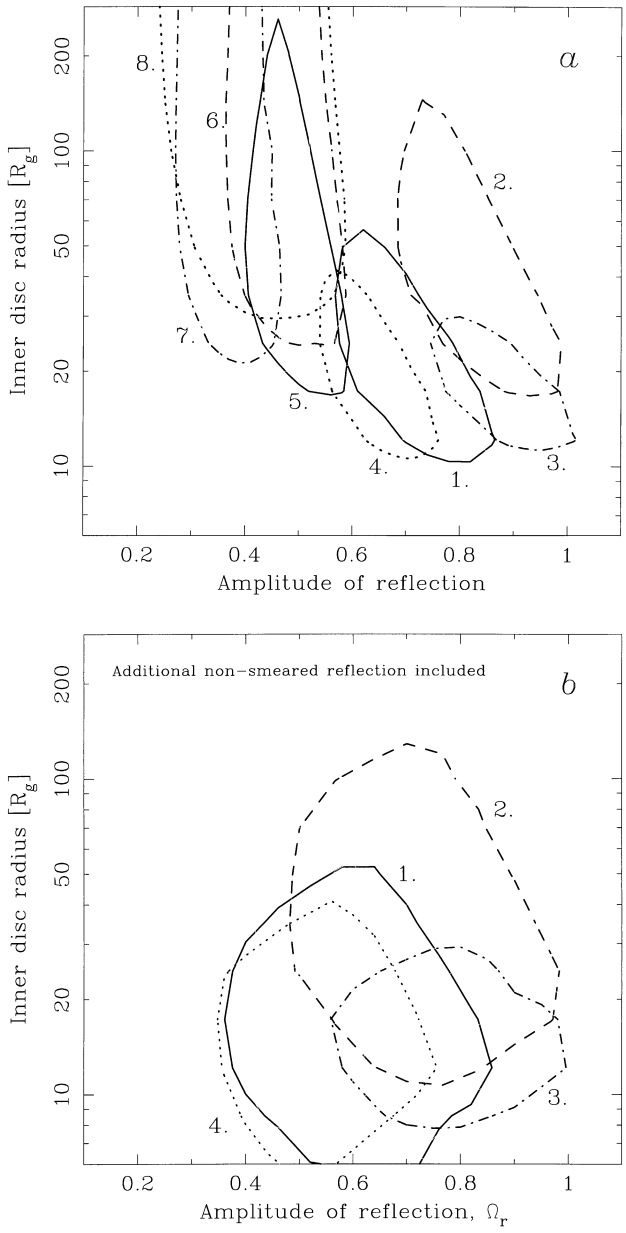

Figure 5. Contours of $\Delta\chi^2 = 4.61$ (90 per cent confidence limits for two parameters) as a function of the amplitude of the smeared reprocessed component, Ω_r, and the inner disc radius, R_{in}, derived from the relativistic smearing. Labels indicate different data sets (Table 2), from the earliest (June 3) to the last observation (November). Panel *a* shows the contours when only the disc-reflected, smeared reprocessed component is present, while panel *b* shows the same contours when an additional, non-smeared reprocessing is allowed for in the model. The amplitude of that non-smeared component is constrained to be < 0.2. Contours for only the first four data sets are plotted in *b*. Presence of the non-smeared component broadens the acceptable range of parameters of the smeared, disc reflection.

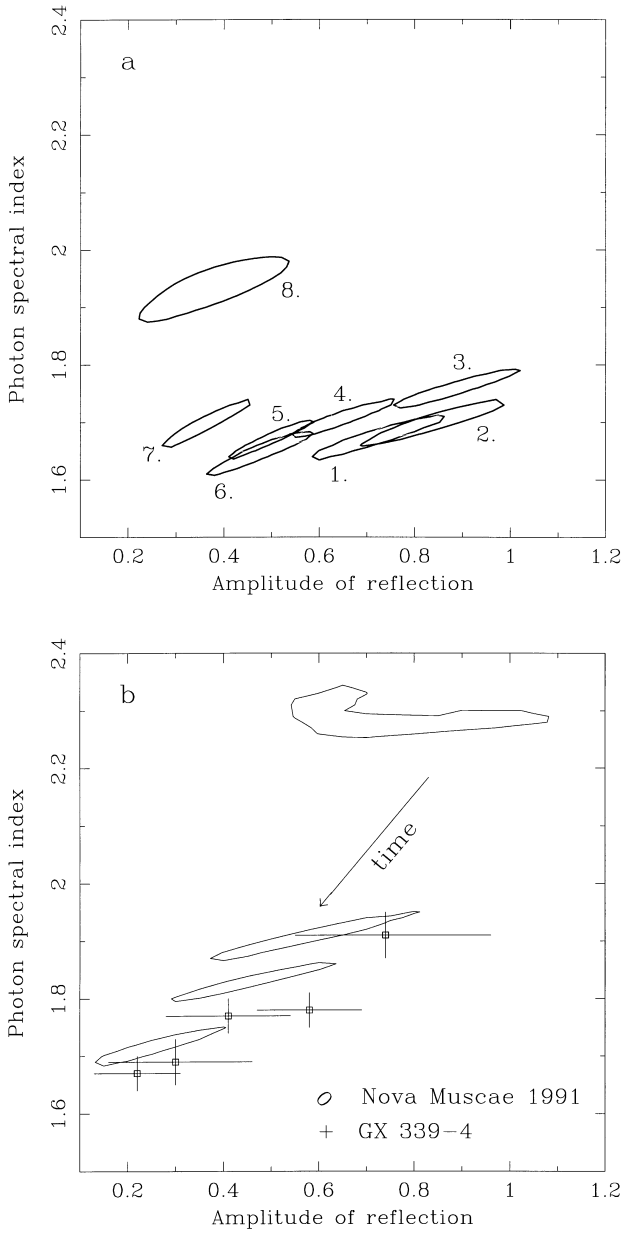

Figure 6. Contours of $\Delta\chi^2 = 4.61$ (90 per cent confidence limits for two parameters) as a function of the amplitude of reflection, Ω_r, and the photon spectral index, Γ, for the decline phase spectra of GS 2023+338 (panel *a*; see Table 2) and (panel *b*) for the soft and hard states of Nova Muscae 1991 (ZDS98) and GX 339-4 (Ueda et al. 1994). The time arrow refers to Nova Muscae only.

evidenced by the rapid spectral variability in the June 3–19 data (see Fig. 2), which can be attributed to photoelectric absorption (Oosterbroek et al. 1997). The reprocessed spectrum coming from this (presumably distant) material would not be relativistically smeared and its presence in the spectrum could mean smaller amplitude of the smeared, disc-reflected component. However, it is also probably not optically thick to electron scattering. The spectra extracted from the extreme right (most absorbed) end of the '$N_H$track' in Fig. 2 give $N_H \approx 4\times10^{23}$ cm^{-2} (see also Oosterbroek et al. 1997). The Compton reflection hump from such a reprocessor is therefore suppressed but the iron Kα line is not, since the optical depth for photoelectric absorption at the Fe K-edge energy is $\sim$1. We have used our Monte Carlo code to simulate reprocessing by such material including the iron line, assuming the reprocessor is not ionized. We then created a table model for XSPEC (parametrized by Γ) and repeated our spectral fitting of the smeared reprocessing including also this additional non-smeared component. The best-fitting contribution of this component is rather small, with $\Omega_{r,non\text{-}smeared} \lesssim 0.01$, but with 90 per cent upper limits ($\Delta\chi^2 = 2.7$) of $\Omega_{r,non\text{-}smeared} = 0.19$, 0.22 and 0.19, for June 3,

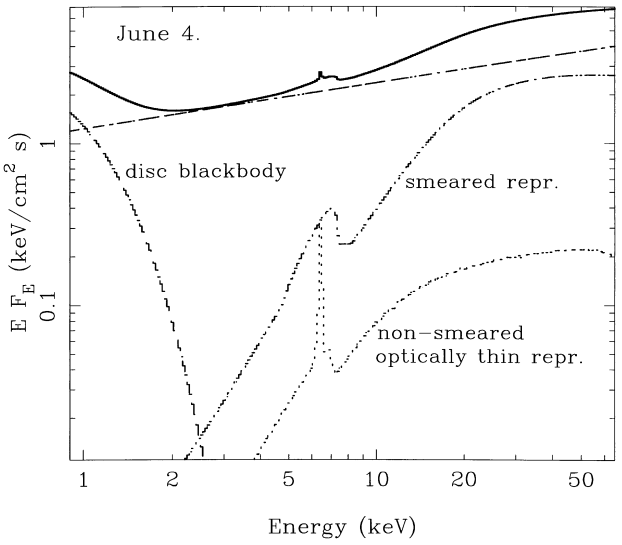

Figure 7. Model spectrum containing an additional, optically thin reprocessed component as fit to the June 4 data set. The amplitude of that reprocessed component is plotted at its 90 per cent upper limit (the best-fitting value is a factor of 10 lower). Such a component, due to reprocessing by cold plasma with $N_{\rm H} \sim 4 \times 10^{23}$ cm^{-2} i.e. $\tau_{\rm es} \sim 0.3$, could be present in the data until June 19. The evidence for presence of such plasma comes from rapid spectral variability which can be modelled as photo–electric absorption (see Figure 2). Suppression of the Compton reflection bump due to $\tau_{\rm es} < 1$ is clearly seen in the model spectrum. Because of that, the required amplitude of the usual, optically thick reprocessing (possibly relativistically smeared) is still high.

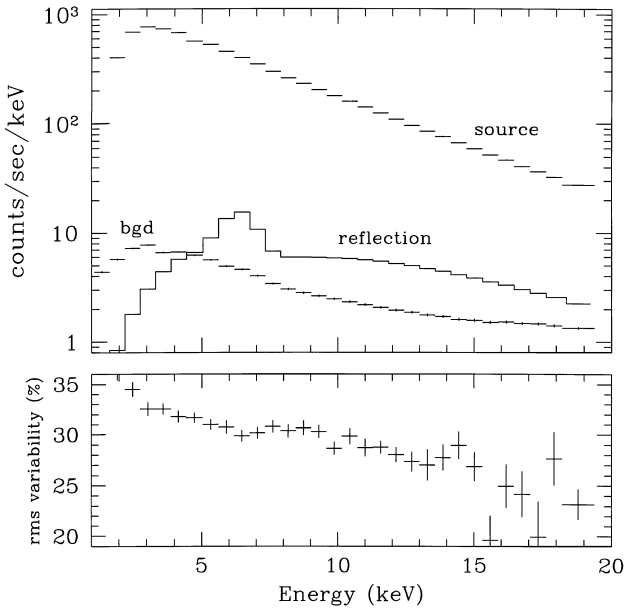

Figure 8. Narrow spectral features in model spectra (e.g. an emission line) are broadened by detector response, so their presence does not manifest as a channel-to-channel change of e.g. rms variability in the observed spectrum. The upper panel shows the count spectrum (i.e. as registered by *Ginga* LAC) of the source on June 10 (data set 3) showing the source, background and possible contribution from the model *non-smeared* reprocessed component (at it 90 per cent upper limit, cf. Fig. 7). Lower panel shows the observed rms variability (computed from non-background-subtracted data).

June 4 and June 10 data sets, respectively. However, this does not substantially change or broaden the allowed ranges of $\Omega_{\rm r}$ of the disc-reflected, smeared component. Fig. 7 shows the model fitted to the June 4 data set, with the contribution from the non-smeared reprocessing at its 90 per cent upper limit, and it shows clearly how the lack of a fully developed Compton hump in the optically thin reflection component cannot contribute much to the observed spectral hardening beyond 10 keV, so as much optically thick reflection is needed as before.

Clearly, the observed (optically thin) absorbing material is insufficient to produce an excess reflected component. We cannot however exclude a priori a possibility of an additional, optically thick reprocessed component being present in the data. Such a component could come from e.g. an outer rim of the accretion disc, since the SS solution predicts that the disc flares in its outer regions.

Solving the SS equations for a vertically integrated, stationary, non-irradiated disc we obtain $\Omega_{\rm r,non\text{-}smeared} \sim H(R = R_{\rm out})/R_{\rm out} \lesssim 0.03$ at $R_{\rm out} = R_{\rm tidal} = 8 \times 10^5\, R_{\rm g}$ (for $\alpha = 0.01$–0.5, $\dot{m} = 0.01$–0.05). Solutions with explicit vertical structure computed by Meyer & Meyer-Hofmeister (1982) give $H/R\,(R_{\rm out}) \sim 0.1$. An irradiated disc would be expected to be more puffed up, but solutions of the vertical structure of irradiated discs depend on details of treatment of the X-ray absorption. Meyer & Meyer-Hofmeister (1982) assumed that all incident X-rays are absorbed and obtained significant thickening of a disc, up to $H/R\,(R_{\rm out}) \sim 0.3$. On the other hand, observational estimates of the optical (disc reprocessed) emission in low mass X–ray binaries also seem to imply $H/R \sim 0.2$ (de Jong, van Paradijs & Augusteijn 1996).

We therefore added a cold ($\xi = 0$), non-smeared reprocessed component (continuum with iron Kα line) to our basic model and we repeated fits to the first four data sets. In view of the above discussion, we set an upper limit of 0.2 to its amplitude. We found that a substantial contribution from such a component is indeed allowed by the data. Consequently, the contribution of the smeared component can be smaller. The results in the $\Omega_{\rm r}$–$R_{\rm in}$ plane for the *relativistic* reprocessing now allow for almost constant $R_{\rm in}$ and $\Omega_{\rm r}$ (Fig. 5b).

Any reprocessed component coming from the distant outer rim of the disc should be constant or only slowly variable. Given that the reflected spectrum is hard, then this should reduce the amount of variability seen at high energies, and around the narrow iron line. Oosterbroek et al. (1997) show that there is no obvious effect at the iron-line energy for any of the decline spectra (although there is a marked constant iron-line component during the outburst). However, this does not rule out the amount of unsmeared reprocessing required here. Fig. 8 shows the June 10th data set, together with the maximum contribution from the non-smeared reflection. Even though the line is intrinsically narrow, it is broadened by the response of the detector. At the iron-line energy the narrow component contributes only 3 per cent of the counts, so its effect on the variability is small. Fig. 8 also shows the observed 0.01–8 Hz rms variability spectrum of the June 10 data, showing that the variability pattern cannot rule out the possible presence of an unsmeared, constant reflected component with $\Omega_{\rm r,non\text{-}smeared} \sim 0.2$.

We are left then with the far from satisfactory situation where GS 2023+338 shows a very different behaviour to that of other SXT. Either it has a remarkable outer disc, which subtends a surprisingly large solid angle, or the source is somehow able to maintain a constant hard X-ray spectral shape despite there being a copious and changing amount of soft photons from the nearby accretion disc.

7 DISCUSSION

The results from the amplitude of reflection and amount of relativistic smearing imply that the disc does not extend down to

the last stable orbit at $6\,R_{\rm g}$. An independent estimate of the inner disc radius could in principle be obtained from the amplitude of the thermal emission, which is proportional to the emitting area. The amplitude is not always well constrained for our data because only the Wien cut-off is within the *Ginga* Large Area Counter (LAC) bandpass for the observed temperatures. In those cases where the amplitude is well constrained the inner radius can be computed from

$$D_{\rm in} = D_{10}\sqrt{\frac{K}{\cos i}}\left(\frac{T_{\rm col}}{T_{\rm eff}}\right)^2 \quad [\rm km],$$

where K is the normalization of the `diskbb` model in XSPEC, D_{10} is the distance to the source in units of 10 kpc, i is the inclination angle and $T_{\rm col}/T_{\rm eff}$ is the ratio of colour to effective temperatures, usually in the range of 1.5–1.9 (e.g. Shimura & Takahara 1995).

The inferred inner disc radius ($D_{\rm in}$ in Table 2 – NB values shown are computed without the colour temperature correction) is compatible with that inferred from relativistic smearing until June 19th. $D_{\rm in}$ is smaller than $R_{\rm in}$ afterwards, although the presence of a disk blackbody component of amplitude corresponding to $D_{\rm in} = R_{\rm in}$ cannot be excluded, if its temperature was below $\sim$0.18 keV, again due to limited bandpass of the LAC detector.

The fact that $D_{\rm in}$ and $R_{\rm in}$ are in agreement is not easily compatible with strong constraints on ionization of the reprocessor. Throughout the entire decline phase the reflecting material had to be very weakly ionized, with a typical upper limit on the mean ionization stage of iron <Fe V. Even assuming a strong radial distribution of ionization, $\xi(r) = \xi(R_{\rm in})\,(r/R_{\rm in})^{-4}$, and allowing for the additional non-smeared and cold reprocessing (Section 6.1), we obtain the highest allowed Fe ionic stage of Fe XVI. This corresponds to the reprocessor temperature $< (2-4)\times 10^5$ K $\approx 20-40$ eV, largely independent of whether iron ionization is in local thermodynamic equilibrium conditions (e.g. Rybicki & Lightman 1979) or photoionization dominates (fig. 2 in Życki & Czerny 1994), and significantly smaller than the temperature of the observed soft emission.

The observed (weakly significant) increase of ξ in July and November data is not consistent with a stationary SS disc, since the latter solution predicts a weaker $\dot{m}$ dependence of the density $n(\dot{m}) \propto \dot{m}^{11/20}$ than $L_{\rm X}(\dot{m})$ which presumably is $\propto\dot{m}$, hence $\xi(\dot{m}) \propto \dot{m}^{9/20}$ should decrease as $\dot{m}$ decreases. Similarly, radial dependence of the density, $\propto r^{-15/8}$ is slower than that of the irradiating flux, $\propto r^{-3}$. This may mean that the disc is not in a steady state; instead the disc may have returned to a cold, low-viscosity state in its outer region where a mass build-up has begun, cutting off the supply of mass to the inner disc and causing departure from the stationary solution for the inner disc. However, solving the vertically averaged SS disc equations (for an un-irradiated disc) we find that hydrogen recombines only beyond $r \sim 10^5\,R_{\rm g}$ when $\dot{m} \sim 10^{-3}\,\dot{M}_{\rm Edd}$, and so the stationary disc solution should be valid at the much closer radii where the reflection comes from.

The power-law spectral index in the last data set (November, 155 days after outburst) is significantly steeper than earlier ($\Gamma \sim 1.9$ versus $\Gamma \sim 1.7$; Table 2). Since the source luminosity at that time was $\sim 3\times 10^{-4}\,L_{\rm Edd}$ it may seem that the source was close to quiescence and consequently its emission was dominated by (Comptonized) synchrotron radiation, as in ADAF-based model of Narayan, Barret & McClintock (1997), and comparable to what was observed by *ASCA*. However, we do see the reprocessed component with $\Omega_{\rm r} \sim 0.3$ so, consequently, the emission should be dominated by Comptonization of the soft photons owing to thermalized irradiation, if the reflection was indeed from the inner disc. Alternatively, again a significant contribution from the outer disc is a possibility, with no feedback of soft photons to the X-ray source. However, the required magnitude of disc flaring is again rather larger than expected. We also note that if the outer disc contribution to reprocessing is dominant at the end of the decline phase, then the overall decrease of $\Omega_{\rm r}$ has to be attributed to the decrease of the smeared component, again raising the problem of the unchanging spectral shape.

8 CONCLUSIONS

Our results support growing evidence that the geometry of accretion flow evolves as the accretion rate changes during the decline of SXT. The evolution involves a retreat of the inner, optically thick disc as indicated by both decreasing amplitude of the reprocessed component and the relativistic smearing becoming less or insignificant (Paper I; ZDS98). These variations of geometry, observed also in persistent source Cyg X-1 (Done & Życki 1998) are usually correlated with spectral states: a small inner disc radius corresponds to soft spectra whilst a large radius corresponds to hard spectra (Nova Muscae 1991, ZDS98). This correlation is easily understood in terms of a scenario where the availability of soft seed photons for Comptonization, determined by the inner disc radius, regulates the Compton cooling and, consequently, the spectral shape (Esin et al. 1997).

However, while GS 2023+338 showed the same receding inner disc, its hard X-ray continuum spectral shape remained largely constant. This poses serious problems to any model involving Comptonization as a source of hard X-rays, and in which changes in the spectral properties are linked to the geometry of accretion.

ACKNOWLEDGMENTS

CD acknowledges support from a PPARC Advanced Fellowship. Work of PTZ was partly supported by grant no. 2P03D00410 of the Polish State Committee for Scientific Research.

REFERENCES

Arnaud K. A., 1996, in Jacoby G., Barnes J., eds, ASP Conf. Ser. Vol. 101, Astronomical Data Analysis Software and Systems V. Astron. Soc. Pac., San Francisco, p. 17
Cui W., Zhang S. N., Focke W., Swank J. H., 1997, ApJ, 484, 383
de Jong J. A., van Paradijs, J., Augusteijn T., 1996, A&A, 314, 484
Done C., Mulchaey J. S., Mushotzky R. F., Arnaud K. A., 1992, ApJ, 395, 275
Done C., Życki P. T., 1998, MNRAS, in press
Dove J. B., Wilms J., Maisack M., Begelman M. C., 1997, ApJ, 487, 759
Ebisawa, K. et al., 1994, PASJ, 46, 375
Esin A. A., 1997, ApJ, 482, 400
Esin A. A., McClintock J. E., Narayan R., 1997, ApJ, 489, 865
Esin A. A., Narayan R., Cui W., Grove J. E., Zhang S.-N., 1998, ApJ, 505, 854
Fabian A. C., Rees M. J., Stella L., White, N. E., 1989, MNRAS, 238, 729
Frank J., King A. R., Raine D., 1992, Accretion Power in Astrophysics. Cambridge University Press, Cambridge
George I. M., Fabian A. C., 1991, MNRAS, 249, 352
Gierliński M., Zdziarski A. A., Done C., Johnson W. N., Ebisawa K., Ueda, Y., Haardt F., Phlips, F., 1997a, MNRAS, 288, 958
Gierliński M., Zdziarski A. A., Dotani T., Ebisawa K., Jahoda K., Johnson W. N., 1997b in Dermer C. D., Strickman M. S., Kurfess J. D., eds, Proc. Fourth Compton Symp. Am Inst. Phys., New York, p. 844

Hayashida K., Inoue H., Koyama K., Awaki H., Takano S., 1989, PASJ, 41, 373
Kaastra J. S., Mewe R., 1993, A&AS, 97, 443
King A. R., 1998, MNRAS, 296, L45
King A. R., Kolb U., Szuszkiewicz E., 1997, ApJ, 488, 89
King A. R., Ritter H., 1998, MNRAS, 293, L42
Kitamoto S., Tsunemi H., Miyamoto S., Yamashita K., Mizobuchi S., 1989, Nat, 342, 518
Magdziarz P., Zdziarski A. A., 1995, MNRAS, 273, 837
Matt G., Perola G., Piro L., 1991, A&A, 247, 25
Meyer F., Meyer-Hofmeister E., 1981, A&A, 104, L10
Meyer F., Meyer-Hofmeister E., 1982, A&A, 106, 34
Miyamoto S., Kitamoto S., Iga S., Negoro H., Terada K., 1992, ApJ, 391, L21
Morrison R., McCammon D., 1983, ApJ, 270, 119
Mitsuda K. et al., 1984, PASJ, 36, 741
Narayan R., 1997, in Wickramasinghe D. T. et al., eds, Proc. IAU Colloq. 163, Accretion Phenomena & Related Outflows. Astron. Soc. Pac., San Francisco, p. 75
Narayan R., Barret D., McClintock J. E., 1997, 482, 448
Nowak M., 1995, PASP, 107, 120
Oosterbroek T. et al., 1996, A&A, 309, 781
Oosterbroek T. et al., 1997, A&A, 321, 776
Osaki Y., 1996, PASP, 108, 39
Poutanen J., 1998, in Abramowicz M. A., Björnsson G., Pringle J. E., eds, Theory of Black Hole Accretion Discs. Cambridge University Press, Cambridge, p. 100
Poutanen J., Krolik J. H., Ryde F., 1997, MNRAS, 292, L21
Reilman R. F., Manson S. T., 1979, ApJS, 40, 815
Revnivtsev M. et al., 1998, A&A, 331, 557
Rybicki G. B., Lightman A. P., 1979, Radiative Processes in Astrophysics. Wiley, New York
Shahbaz T., Ringwald F. A., Bunn J. C., Naylor T., Charles P. A., Casares J., 1994, MNRAS, 271, L10
Shakura N. I., Sunyaev R. A., 1973, A&A, 24, 337
Shimura T., Takahara F., 1995, ApJ, 445, 780
Smak J. I., 1982, Acta Astron., 32, 199
Tanaka Y., Lewin W. H. G., 1995, in Lewin W. H. G., van Paradijs J., van den Heuvel E., eds, X-Ray Binaries. Cambridge University Press, Cambridge, p. 126
Tanaka Y., Shibazaki N., 1996, ARA&A, 34, 607
Ueda Y., Ebisawa K., Done C., 1994, PASJ, 46, 107
van Paradijs J., 1996, ApJ, 464, L139
Witt H. J., Czerny B., Życki P. T., 1997, MNRAS, 286, 848
Życki P. T., Czerny B., 1994, MNRAS, 266, 653
Życki P. T., Done C., Smith D. A., 1997, ApJ, 488, L113 (Paper I)
Życki P. T., Done C., Smith D. A., 1998, ApJ, 496, L25 (ZDS98)

APPENDIX A RADIAL DEPENDENCE OF IRRADIATION EMISSIVITY

The irradiation emissivity follows closely the r^{-3} dependence if the reflecting disc is outside a central source of radiation, except very close to the source. Consider a spherical source, centred on the black hole, of maximum radius R_0, with the disc extending outside it, i.e. from $r = R_0$ to $R_{\rm out} \gg R_0$. We allow for a flaring disc with height described by an arbitrary function $h(r)$. Introducing a spherical coordinate system in the usual manner (see Fig. A1) we have:

$$\mathrm{S} = [\rho\ \sin\theta\ \cos\phi, \rho\ \sin\theta\ \sin\phi, \rho\ \cos\theta],$$

$$\mathrm{D} = [0, r, h(r)].$$

The vector normal to the disc surface is

$$\boldsymbol{n} = \left[0, -\frac{\mathrm{d}h}{\mathrm{d}r}, 1\right].$$

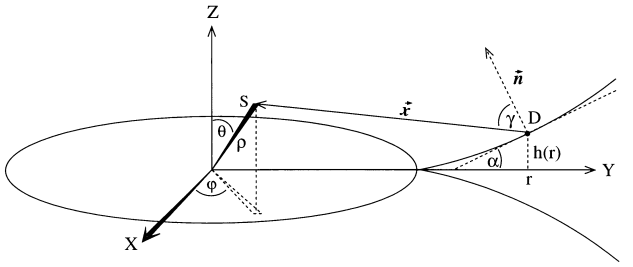

Figure A1. Geometry of disc irradiation. The X-ray source is assumed spherical, with outer radius R_0. The disc extends from R_0 to $R_{\rm out} \gg R_0$. S is an arbitrary point within the source while D is a point on the disc surface. Note that the X-ray source is plotted in perspective but a cut in the y–z plane for the disc is used.

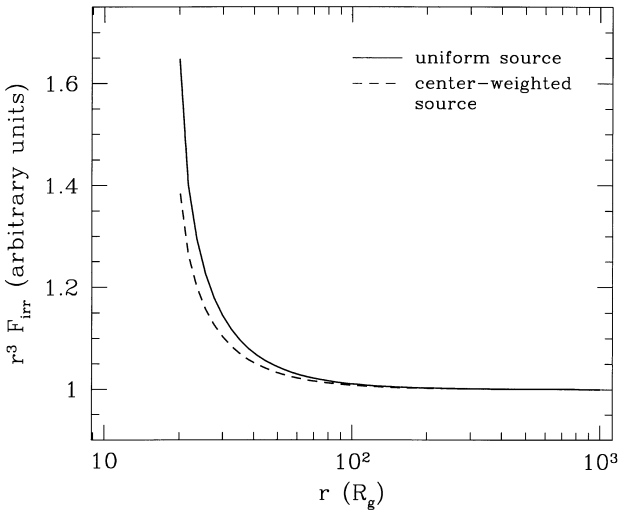

Figure A2. Irradiation emissivity, $r^3 F_{\rm irr}(r)$, for a central, spherical source illuminating an external, flat disc. Inner source radius is assumed $6R_{\rm g}$, outer one $20R_{\rm g}$, from where the disc extends outwards. The emissivity is somewhat steeper than r^{-3} for $r < 100R_{\rm g}$ and its shape depends on how strongly the luminosity inside the source is concentrated towards the centre. The solid curve shows the emissivity for a uniform source, whilst the dashed curve is for the luminosity per unit volume $r^{-4}(1 - \sqrt{6/r})$. In the $20 - 40R_{\rm g}$ range the approximate power-law fit to $F_{\rm irr}(r)$ has a slope equal to $\beta = 3.5$ in the former case, while $\beta = 3.3$ in the latter.

The distance between S and D is the length of the vector from S to D, $l \equiv |\boldsymbol{x}|$,

$$l^2 = \rho^2 + r^2 - 2\rho r \sin\theta \sin\phi + h(r)[h(r) - 2\rho\cos\theta], \qquad \text{(A1)}$$

while the cosine of the illumination angle is

$$\cos\gamma = \boldsymbol{n}\cdot\boldsymbol{x}/(|\boldsymbol{n}||\boldsymbol{x}|) = \frac{\frac{\mathrm{d}h}{\mathrm{d}r}(r - \rho\sin\theta\sin\phi) + \rho\cos\theta - h(r)}{l\sqrt{1 + (\mathrm{d}h/\mathrm{d}r)^2}}. \qquad \text{(A2)}$$

Contribution to the irradiation emissivity is thus

$$\delta F_{\rm irr} = \mathrm{d}V\ \cos\gamma/l^2, \qquad \text{(A3)}$$

where $\mathrm{d}V = \rho^2\ \sin\theta\,\mathrm{d}\rho\,\mathrm{d}\theta\,\mathrm{d}\phi$ is the volume element of the source. Neglecting radiative transfer and relativistic effects within the source, we obtain the emissivity by integrating $\delta F_{\rm irr}$ over the source,

$$F_{\rm irr}(r) = \int f(\boldsymbol{r})\,\delta F_{\rm irr},$$

where $f(\boldsymbol{r})$ describes the distribution of volume emissivity within the source.

Examples of $F_{\rm irr}(r)$ are plotted in Fig. A2. As can be seen close to the source the emissivity can deviate from the r^{-3} dependence. It is generally steeper ($r^{-\beta}$ with $\beta > 3$) owing to the finite size of the source. The magnitude of deviation depends on the luminosity distribution within the source. The stronger the central concentration of luminosity, the weaker the deviations.

A special case of a point source located on the symmetry axis, above a disc, is recovered from equations (A1) and (A2) assuming polar angle $\theta = 0$. Assuming further a flat disc [$h(r) = 0$] we obtain the well-known formula,

$$F_{\rm irr}(r) \propto \frac{1}{\left(r^2 + h_{\rm s}^2\right)^{3/2}} \simeq r^{-3} \text{ for } r \gg h_{\rm s},$$

where $h_{\rm s}$ is the height of the source above the disc plane.

Another frequently quoted formula for the irradiation temperature in a flaring disc (SS; van Paradijs 1996; King et al. 1997), results from our formulae (A1) and (A2) in the limiting case of $\rho = 0$, putting $l = r$ (i.e. it is equivalent to assuming $r \gg R_0$) and neglecting dh/dr in the denominator of (A2).

Our formulae (A1)–(A3) could also in principle be applied to a disc extending *inside* the source. A simpler way to find the irradiation emissivity in this case is to notice that $F_{\rm irr}(r)$ follows the local electron emission, vertically integrated over the hot source, q^-. This generally follows the viscous energy generation in the hot source which however is not necessarily described by the usual dependence $q^+ \propto r^{-3}$. First, the ratio of $q^+_{\rm hot}/q^+_{\rm tot}$ can be a function of radius (Witt, Czerny & Życki 1997). Secondly, a fraction f of $q^+_{\rm hot}$ can be advected, and f itself can be a function of radius. Thirdly, Compton cooling by non-local soft photons can have a strong effect (Esin 1997), especially in the transition region. Since the non-local cooling enhances electron emission (Esin 1997), we can expect $F_{\rm irr}(r)$ to be steeper than r^{-3} i.e. $\beta > 3$ close to the inner disc radius. All the above effects are model-dependent and need to be properly modelled.

This paper has been typeset from a TEX/LATEX file prepared by the author.